Figure S1

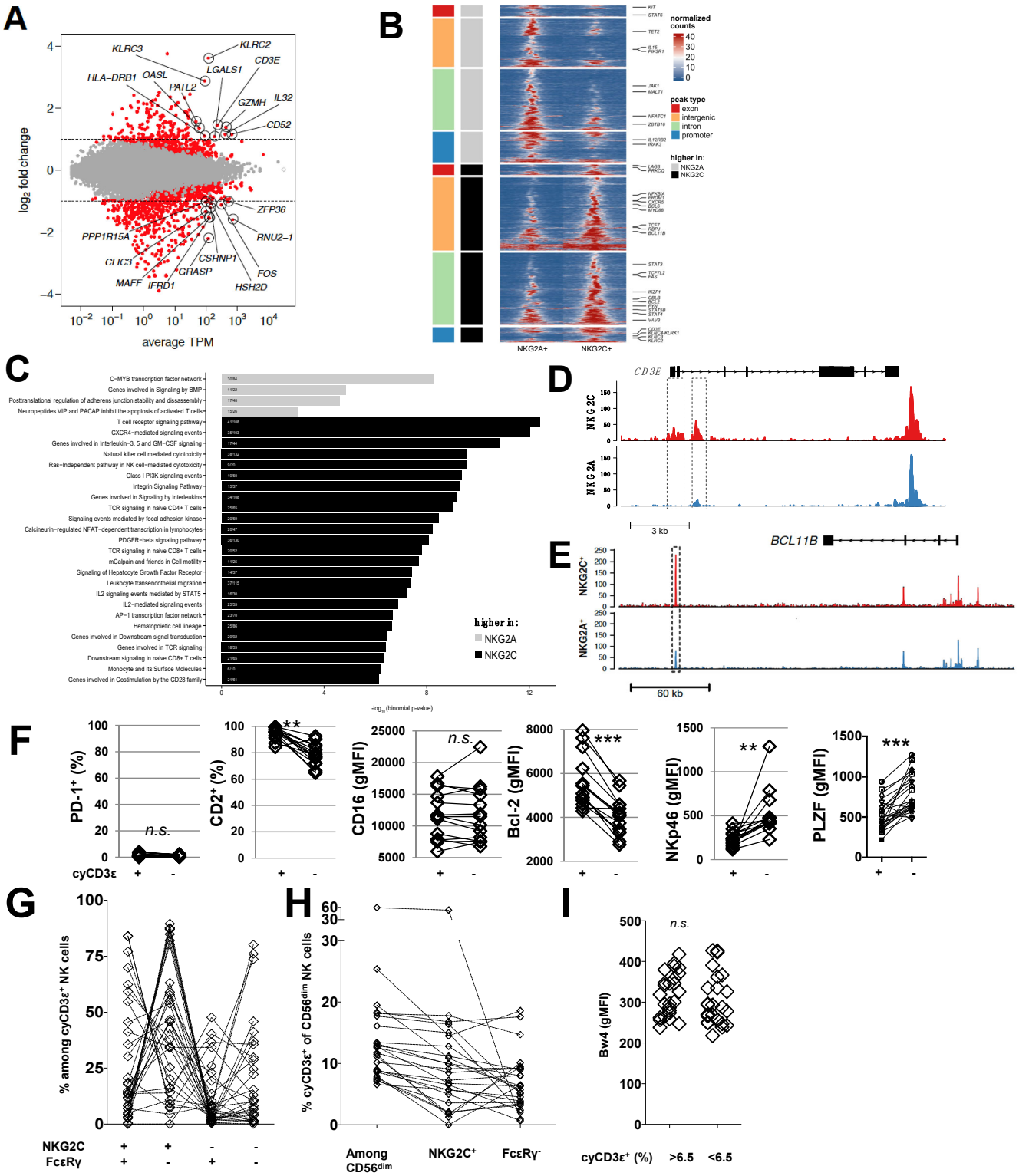

Fig. S1. A to E: Integrated transcriptomic and epigenomic profiling of NKG2C$^+$ and NKG2A$^+$ NK cells from HCMV-seropositive donors. (A) MA plot depicts average transcripts-per-million (TPM) over a log10 scale on x-axis and log2 fold change on y-axis. Red dots highlight DE (FDR-adjusted $p < 0.05$) genes when comparing NKG2C$^+$ versus NKG2A$^+$ NK cells. Highlighted are top 10 DE genes ranked by TPM that show higher than a log2 FC of 1 in either direction. Dotted vertical and horizontal lines mark FC at +/- 1. Diamond signifies gene with capped TPM value. (B) Heatmaps (right) of chromatin accessibility measured by ATAC-seq, with each row representing a peak. Heatmap is split by peak categories as demarcated by color blocks (left). Categories are defined by whether they show increased accessibility in NKG2C$^+$ or NKG2A$^+$ NK cells and by peak type. (C) Bar plot of $-\log_{10}$(p-values) calculated from gene ontology enrichment analysis. Depicted are all or top 25 pathways enriched among genes associated with peak regions showing higher accessibility in NKG2C$^+$ (black) or NKG2A$^+$ (gray) NK cells. Numbers within bar plot show fraction of DA genes out of the total gene set. (D) Genomic tracks of mapped ATAC-seq reads at the *CD3E* locus, with dashed lines indicating DA peak regions. The *y*-axis depicts normalized counts, while the *x*-axis displays genomic axis with scale bar. (E) Genomic tracks of mapped ATAC-seq reads at the *BCL11B* locus, with dashed box indicating a differentially accessible (DA) peak region when comparing NKG2C$^+$ to NKG2A$^+$ NK cells. y-axis depict normalized counts, while x-axis displays genomic axis with scale bar. FDR = false discovery rate; FC = fold change. **F to I: Phenotype of CD3ε$^+$ NK cells in healthy donors.** (F) Percentages or geometric mean fluorescence intensity (gMFI) of PD-1, CD2, CD16, Bcl-2, NKp46, and PLZF on cyCD3ε$^+$ NK cells and cyCD3ε$^-$ NK cells from each donor. Populations from the same donors are paired. (G) Frequencies of NKG2C$^+$FcεRIγ$^+$, NKG2C$^+$FcεRIγ$^-$, NKG2C$^-$FcεRIγ$^+$, and NKG2C$^-$FcεRIγ$^-$ NK cells among cyCD3ε$^+$ NK cells are shown. (H) Frequencies of cyCD3ε$^+$NKG2C$^+$ and cyCD3ε$^+$FcεRIγ$^-$ NK cells among CD56^{dim} NK cells are shown (n=25). (I) Geometric mean fluorescence intensity (gMFI) of HLA-Bw4 on lymphocytes from donors grouped based on cyCD3ε expression is shown.

Figure S2

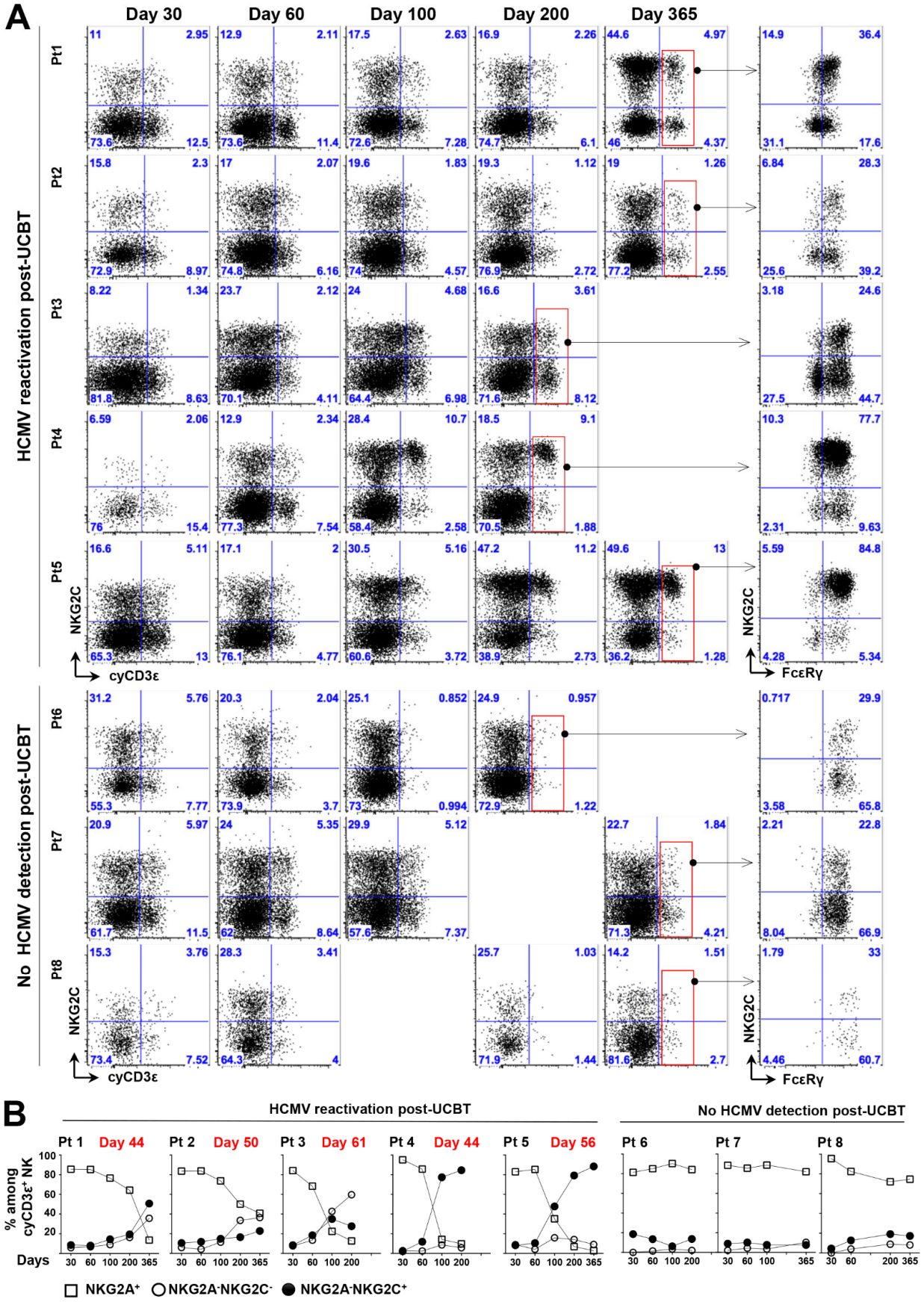

Fig. S2. Detection of cyCD3ε$^+$ NK cells in UCBT recipients. (A) Surface expression of NKG2C and intracellular expression of CD3ε and FcεRIγ in total NK cells from UCBT recipients at indicated timepoints post-UCBT. (B) Expression of NKG2A and NKG2C on cyCD3ε$^+$ NK cells from UCBT patients with or without HCMV reactivation post-transplant. The percentages of NKG2A$^+$ (open square) or NKG2A$^-$NKG2C$^-$ (open circle) or NKG2A$^-$NKG2C$^+$ (black circle) cells among cyCD3ε$^+$ NK cells were evaluated. The day of HCMV reactivation post-UCBT is indicated.

Figure S3

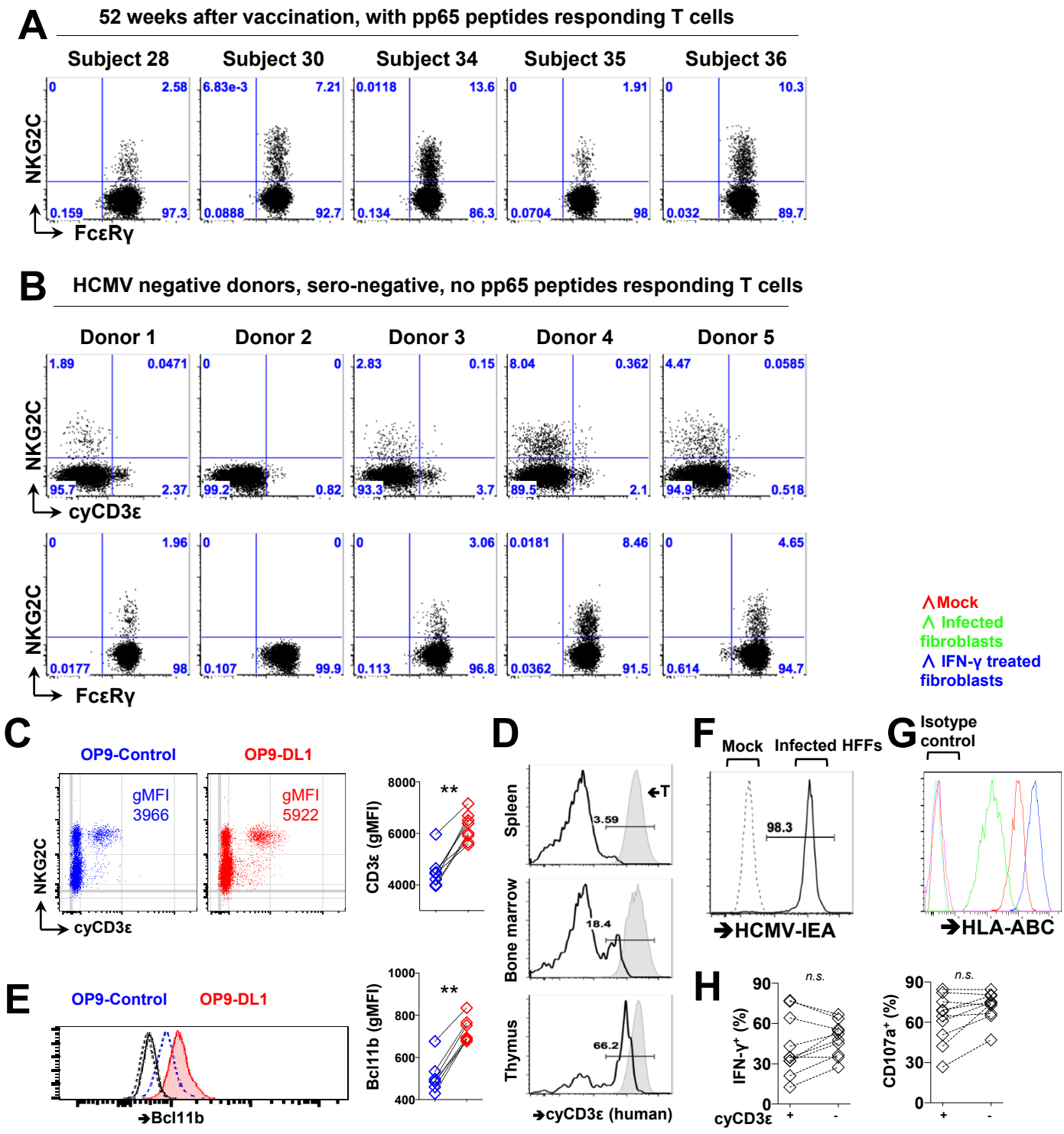

Fig. S3. A and B: Detection of HCMV-induced NK cells in fibroblast-adapted HCMV vaccines infected subjects and HCMV-seronegative donors. Expressions of NKG2C, cyCD3ε, and FcεRIγ among CD56^{dim} NK cells from (A) vaccinated subjects at one-year post-vaccination and (B) HCMV-seronegative donors. **C to E: Bcl11b and is a target of Notch signaling** (**C**) NK cells were purified from cyCD3ε^{+} NK cell positive donors and incubated with OP9 cells or OP9-DL1 cells. The gMFI of CD3ε was evaluated among cyCD3ε^{+} NK cell (n=8). One representative HCMV seropositive donor whose NK cells of cyCD3ε expression overlap with NKG2C expression is shown. Data are representative of two independent experiments with the same results. (D) Human cyCD3ε expression among murine NK cells isolated from indicated organs harvested from human CD3ε transgenic F1 heterozygotes mice. (E) Bcl11b expression of purified NK cells after culture with parental OP9 cells (open blue) or OP9-DL1 cells (red tint) was shown. Isotypes are shown in black lines. **F to H: CyCD3ε^{+} NK cells response to cell targets.** (F) Mock infected fibroblasts (dashed) or HCMV infected fibroblasts (solid) were stained with anti-HCMV IEA antibody. (G) Surface expression of HLA-ABC on HCMV infected fibroblasts (green), non-infected fibroblasts (red), and IFN-γ treated non-infected fibroblasts (blue) is shown with isotype controls. (H) CD107a and IFN-γ responses were assessed in cyCD3ε^{+} and cyCD3ε^{-} NK cells against K562 cells. Responses of cyCD3ε^{+} or cyCD3ε^{-} populations from the same individual are paired (n=10).

Figure S4

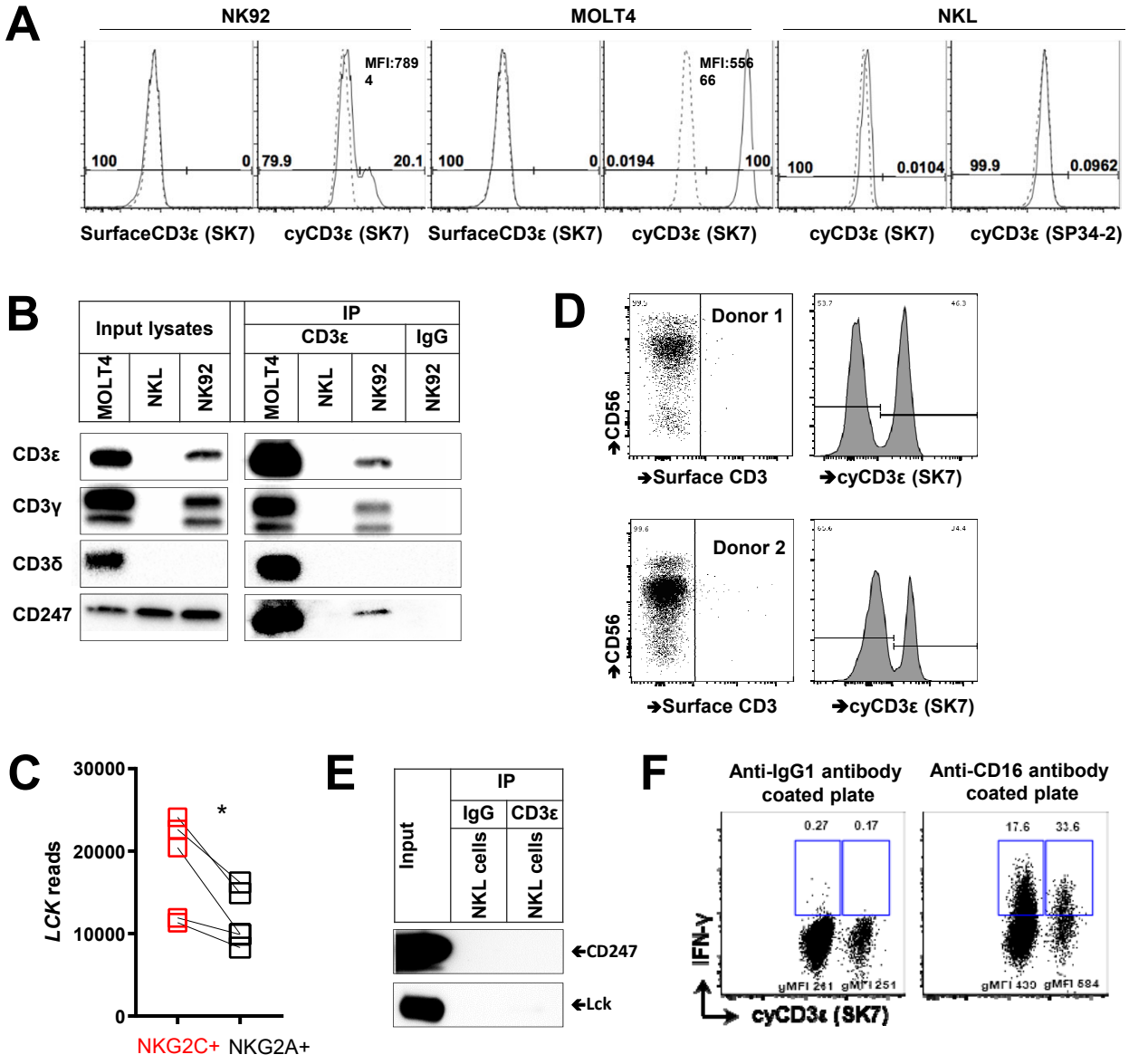

Fig. S4. Detection of cyCD3ε among cell lines. (A) Surface and intracellular expression of CD3ε in NK92, MOLT4, and NKL cells. Isotype controls are indicated in dashed lines. (B) MOLT4, NKL, and NK92 cells were lysed and immunoprecipitated with control IgG or anti-CD3ε antibodies and blotted using anti-CD3ε, anti-CD3γ, anti-CD3δ, and anti-CD247. Results are representative of two independent experiments. (C) *LCK* raw counts of NKG2A$^+$ and NKG2C$^+$ NK cells were shown. Paired symbols indicate populations from the same donor. (D) The purity of NK cells used for immunoprecipitation from cyCD3ε$^+$ NK cell donors were shown. (E) NKL cells were lysed, and immunoprecipitated with control IgG or anti-CD3ε antibody for CD247 and Lck detection. (F) CD16$^+$ NK92MI cells were stimulated with anti-CD16 antibody (3G8) or control antibody for 5 hours in the presence of GolgiStop. IFN-γ activity was evaluated in CD3 positive and CD3 negative CD16$^+$ NK92MI cells. The indicated percentages of positive cells in FACS plot were determined as percentage of CD3 positive and CD3 negative NK cells. The gMFIs of IFN-γ were evaluated on the CD3 positive and CD3 negative NK cell populations revealing a higher frequency of responsive cells among the CD3$^+$ population. Plots are representative of two independent experiments, both with similar results.